Electronic Supplementary Information for

Spectroscopic Evidence for a H Bond Network at Y_{356} Located at the Subunit Interface of Active *E. Coli* Ribonucleotide Reductase

Thomas U. Nick,[a] Kanchana R. Ravichandran,[b, ⊥] JoAnne Stubbe*[,b], Müge Kasanmascheff *[, a, †] and Marina Bennati *[, a, c]

[a)] Research Group Electron-Spin Resonance Spectroscopy, Max Planck Institute for Biophysical Chemistry, 37077 Göttingen, Germany.

[b)] Department of Chemistry, Massachusetts Institute of Technology, Cambridge, Massachusetts 02139, United States.

[c)] Department of Chemistry, University of Göttingen, 37077 Göttingen, Germany.

* Corresponding authors.

⊥ Current Address: Moderna Therapeutics, 200 Technology Square, Cambridge, MA 02139, USA
† Current Address: Department of Chemistry and Chemical Biology, Technical University of Dortmund, Otto-Hahn-Str. 6, 44227 Dortmund, Germany

Figure S1A, S1B and S1C: Comparison of RFQ and manual quench EPR spectra recorded at 94 GHz and separation of the EPR signal of trapped radical from that of F_3Y_{122}•-β. A) The rate of formation and disappearance of the Y_{356}• generated upon incubation of F_3Y_{122}•-β2/wt-α2/ATP/CDP was monitored by RFQ-EPR experiments at 94 GHz and 80 K. The proximity of F_3Y_{122}• to the di-iron cluster[1, 2] alters its relaxation properties at 80K so that the Y_{356}• can be monitored directly (**Fig. S1B**). The freeze-quenching times are shown next to each spectrum. The EPR spectrum of a hand-quenched sample (30 s) with its corresponding simulation (black line) is shown for comparison. Simulation parameters are given in **Table S2**. To calculate the percentage of trapped Y_{356}•, the EPR experiments were also recorded at 20 K for each time point (**Fig. S1C**). The **inset** in the figure shows the fit to exponential equation (Eq. 1 in *Experimental* main text) to obtain the rate constants k_1 (7.7 s^{-1}) and k_2 (0.1 s^{-1}). Based on our recent studies, k_1 and k_2 are the rate constants for the forward and reverse PCET, respectively.[3] These values can be compared to the previous studies in H_2O of k_1 = 30 s^{-1} and k_2 = 0.5 s^{-1}.[3] The differences could be due to the protein concentrations, 80 uM and 300 uM in H_2O and D_2O, respectively or they might be attributed to a solvent kinetic isotope effect (KIE) of ~4. Note that D_2O buffer was used to better resolve hf couplings and the *g*-values.[4, 5] **B)** The 94 GHz EPR spectra of the RFQ sample after 0.3 s recorded at 80 K and F_3Y_{122}• recorded at 20 K are shown in green and red, respectively. The absence of the spectral features associated with F_3Y_{122}• in the green spectrum shows that F_3Y_{122}• contribution cannot be detected at 80 K due to its fast relaxation. **C)** The EPR spectra at 20 K of the RFQ sample after 0.3 s and a reference spectrum of F_3Y_{122}• are shown in black and red, respectively. The details of the experimental conditions are given in the main text in *Experimental*. The black spectrum is the composite spectrum of F_3Y_{122}• and Y_{356}•. The subtraction of the red spectrum from the black one results in blue trace that belongs to Y_{356}• solely. The ratio of the integral of the blue trace to that of black trace gives the percentage of the trapped Y_{356}•.

A)

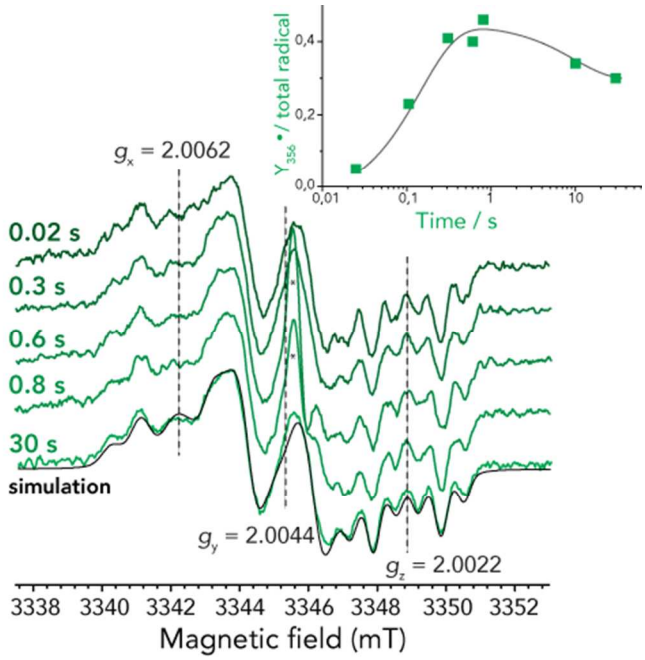
g_x = 2.0062
0.02 s
0.3 s
0.6 s
0.8 s
30 s
simulation
g_y = 2.0044
g_z = 2.0022
3338 3340 3342 3344 3346 3348 3350 3352
Magnetic field (mT)
Y_{356}•/ total radical
0,0
0,2
0,4
0,01
0,1
1
10
Time / s

B)

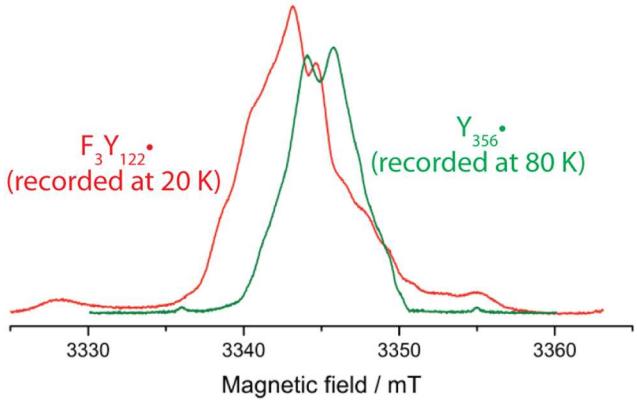
F_3Y_{122}•
(recorded at 20 K)
Y_{356}•
(recorded at 80 K)
3330
3340
3350
3360
Magnetic field / mT

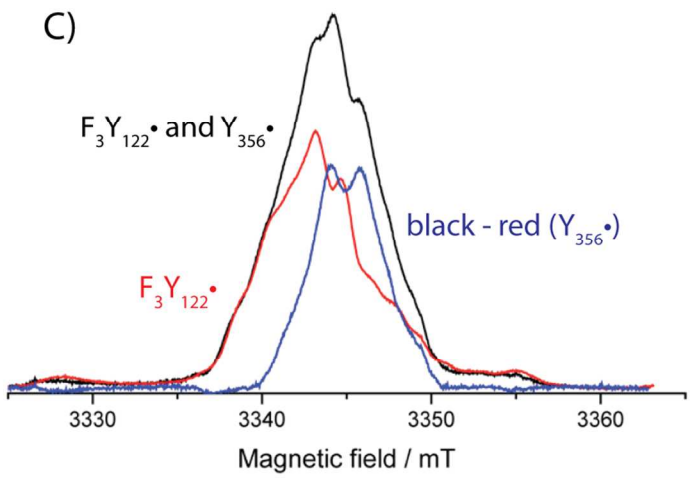
C)
F3Y122• and Y356•
black - red (Y356•)
F3Y122•
3330
3340
3350
3360
Magnetic field / mT

Figure S2: PELDOR/DEER measurements with Y_{356}•(wt-α) at 34 GHz and 40K. A) ESE spectrum recorded at 40 K (violet) is composed of trapped pathway radicals and F_3Y_{122}•. The signal of F_3Y_{122}• does not contribute to the refocused echo at 40 K but it can be excited by the pump pulse. The EPR spectrum of the trapped species shown in red is recorded at 70 K. Detect (D) and pump (P) frequency positions for each PELDOR measurement are displayed by red, blue and green arrows. Detect and pump pulse lengths for these experiments were 20 ns and 18 ns, respectively. Frequency separation between detect and pump pulses was 86 MHz for all data sets. Exp. conditions: shot repetition time = 18 ms, shots/point = 10, number of scans = 500. **B)** Background- and phase-corrected, normalized (time signal V(t) divided by the signal at echo maximum V(t=0)) 34 GHz PELDOR time traces of three experimental setups (1, 2, 3) and the sum of the three traces (**C**) was analyzed by DEER Analysis[6] using Tikhonov regularization.[7] The fittings are overlaid and shown with solid lines. **D)** Distance distribution obtained from the analysis in (**C**) resulted in two distances: (1) 3.05 ± 0.08 nm with 80% ± 5 contribution and (2) 3.86 ± 0.07 nm with 20% ± 5 contribution. Asterisk indicates an artifact attributed to the analysis procedure. This distance changes between 4.3 nm and 5 nm depending on the background subtraction.

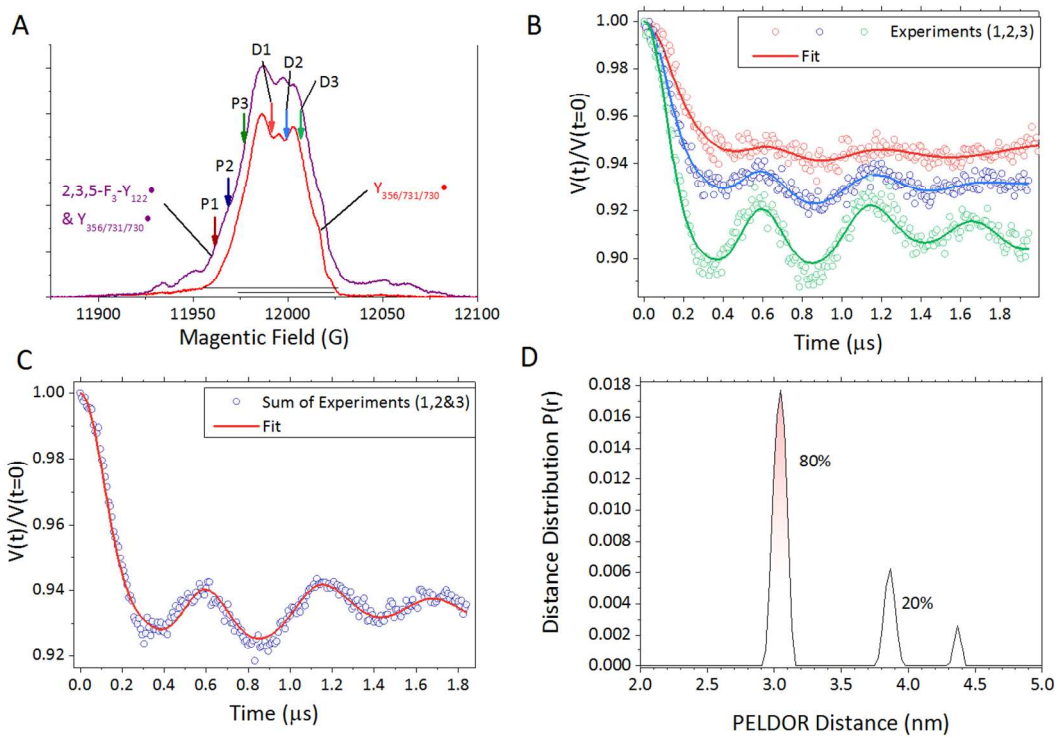

Figure S3: PELDOR/DEER measurements with Y_{356}•(Y_{731}F-α) at 34 GHz and 40K. A) ESE spectrum recorded at 40 K (violet) is composed of Y_{356}• and F_3Y_{122}•. The Y_{356}• spectrum shown in red is recorded at 70 K. Detect (D) and pump (P) frequency positions for each PELDOR measurement are displayed by red, blue and green arrows. D and P pulse lengths for these experiments were 46 ns and 56 ns, respectively. Frequency separation between D and P pulses was 54 MHz for all data sets. Exp. conditions: shot repetition time = 10 ms, shots/point = 50, number of scans = 200. **B)** Background- and phase-corrected, normalized (see Fig. S2) 34 GHz PELDOR time traces of three experimental setups (1, 2, 3) and the sum of the three traces (**C**) was analyzed by DEER Analysis[6] using Tikhonov regularization.[7] The fittings are overlaid and shown with solid lines. **D)** Distance distribution obtained from the analysis in (**C**) resulted in a main distance of 3.04±0.06 nm.

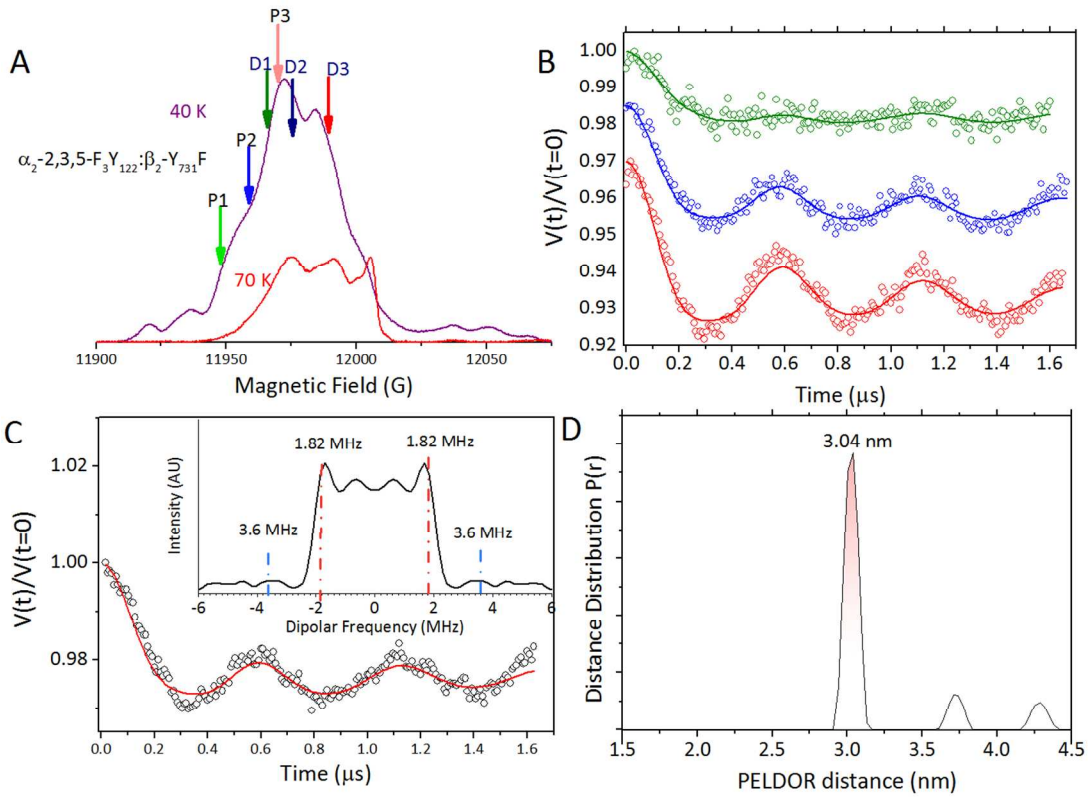

Figure S4: PELDOR/DEER measurements with Y_{356}•(Y_{730}F-α) at 34 GHz and 40K. A) ESE spectrum recorded at 40 K (violet) is composed of trapped pathway radicals and F_3Y_{122}•. The EPR spectrum of the trapped species shown in red is recorded at 70 K. D and P frequency positions for each PELDOR measurement is displayed by orange, blue and green arrows. D and P pulse lengths for these experiments were 12 ns and 24 ns, respectively. Frequency separation between D and P pulses was 90 MHz for all data sets. Exp. conditions: shot repetition time = 18 ms, shots/point = 10, number of scans = 637. **B)** Background- and phase-corrected, normalized 34 GHz PELDOR time traces of three experimental setups (1, 2, 3) and the sum of the three traces (**C**) was analyzed by DEER Analysis[6] using Tikhonov regularization.[7] The fittings are overlaid and shown with solid lines. **D)** Distance distribution obtained from the analysis in (**C**) resulted in a distance of 3.03±0.04 nm.

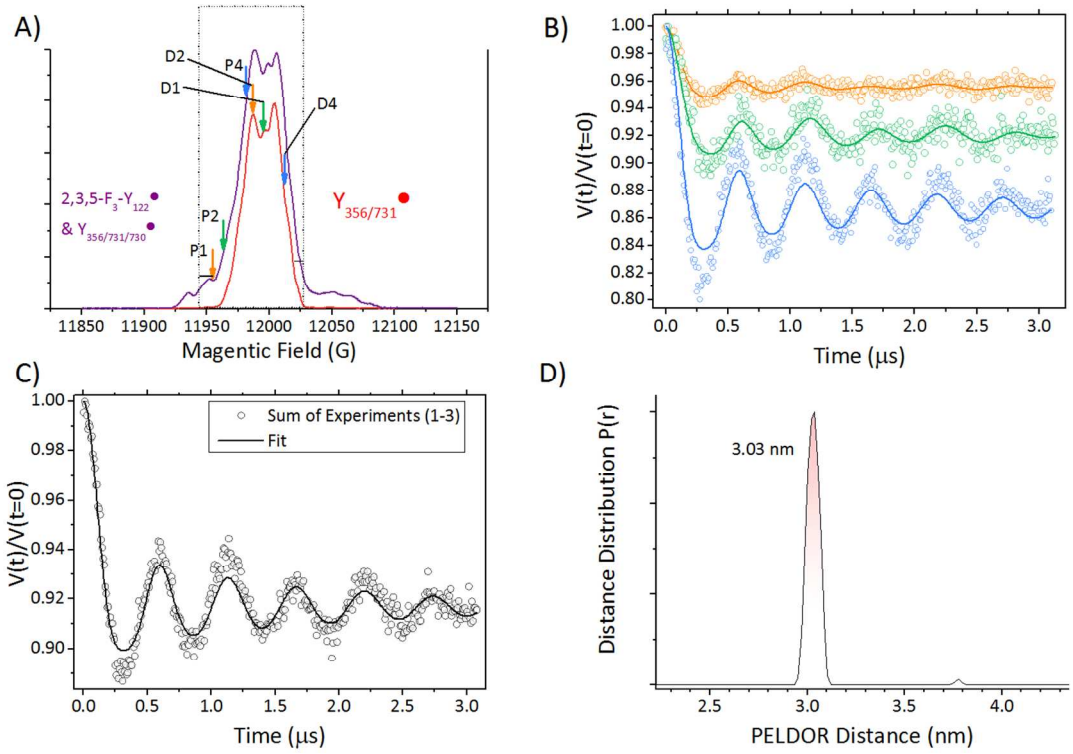

Table S1: Comparison of diagonal distances to Y_{356}•. Summary of diagonal inter spin distances between residue Y_{122} and Y_{356} obtained from the measurements shown in **Fig. S2**, **S3** and **S4** as compared with previous measurements in the literature using β_2-DOPA-Y_{356}[8] or β_2-NO_2Y_{122}[9] as radical traps (hot oxidant, see main text). Numbers in parenthesis give the RFQ times of the reaction. Peak distances are given with their width of distance distributions Δr, which is defined as half width at half peak height. The uncertainty of the main peak distance observed in this work is estimated to be similar to previous experiments with trapped Y•'s, i.e. ± 0.01 nm.[10]

Mutations	Main peak distance ± Δr [nm]	Other observed distances [nm]
β_2-2,3,5-F_3Y_{122}:α_2-wt	3.05 ± 0.08	3.86 ± 0.07
β_2-2,3,5-F_3Y_{122}: α_2-Y_{731}F	3.04 ± 0.06	-
β_2-2,3,5-F_3Y_{122}: α_2-Y_{730}F	3.03 ± 0.04	-
β_2-NO_2Y_{122}:α_2-wt (8 ms)[9]	3.00 ± 0.04	3.81 ± 0.04
β_2-NO_2Y_{122}: α_2-Y_{731}F (8ms)[9]	3.01 ± 0.04	-
β_2-DOPAY_{356}:α_2-wt[8]	3.06 ± 0.05	-

Figure S5: Estimating the ratio of trapped radical species in 263 GHz EPR spectra. The percentage of Y_{356}• trapped in Y_{356}•(wt-α) and Y_{356}•(Y_{730}F-α) was obtained by simulating the $Y_{731/730}$• contribution to the 263 GHz EPR spectrum at 80 K using *g* values of 2.0072, 2.0045, 2.0022 and the hyperfine parameters reported.[9] Experimental conditions were as follows: ESE (π/2–τ–π–echo) spectra: π/2 = 34 ns, τ = 300 ns, 250 averages/point, number of scans (up to down) = 209 and 32 , T = 80 K. Note that, prior to simulation, a small contribution of F_3Y_{122}• (8%) was subtracted based on its characteristic ^{19}F-hyperfine broadening at the low and high field side of the 263 GHz EPR spectrum. Under the assumption of similar T_1 relaxation behavior, the integral of the simulated $Y_{731/730}$• contribution is compared with the integral over the full EPR spectrum. We calculated that the ESE spectra of Y_{356}•(wt-α) and Y_{356}•(Y_{730}F-α) are composite of Y_{356}• (84±3%) and Y_{731}• and/or Y_{730}• (16±3%). The mutant Y_{731}F-α cannot form Y_{731}• and/or Y_{730}•. In these samples we observe a strong contribution (50 %) of a component with *g* values of 2.0072, 2.0045, 2.0022 (Fig. 3, main text), attributed to a second distinct electrostatic environment of Y_{356}• (main text).

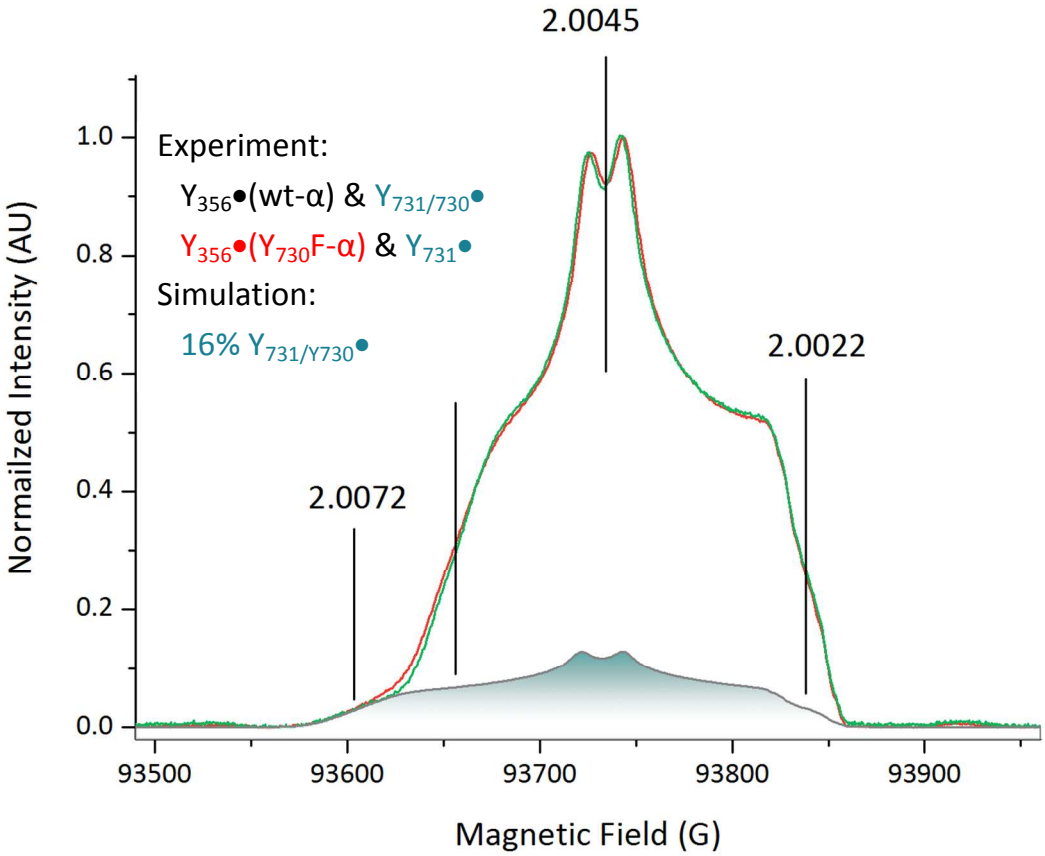

Figure S6: Analysis of 263 GHz spectra. Derivative 263 GHz spectra of Y_{356}•(Y_{731}F-α), Y_{356}•(wt-α) , and Y_{356}•(Y_{730}F-α) are shown in blue, green, and red, respectively. The simulations for the Y_{356}• component are shown below each experimental trace in grey. Experimental conditions are listed in *Experimental* in the main text. The contribution of two Y_{356}• species generated with Y_{731}F-α is shown in orange and blue gradient. The simulation parameters for one of the two species in Y_{356}•(Y_{731}F-α) are kept identical to the parameters used for Y_{356}•(wt-α). The simulation parameters are listed in **Table S2**.

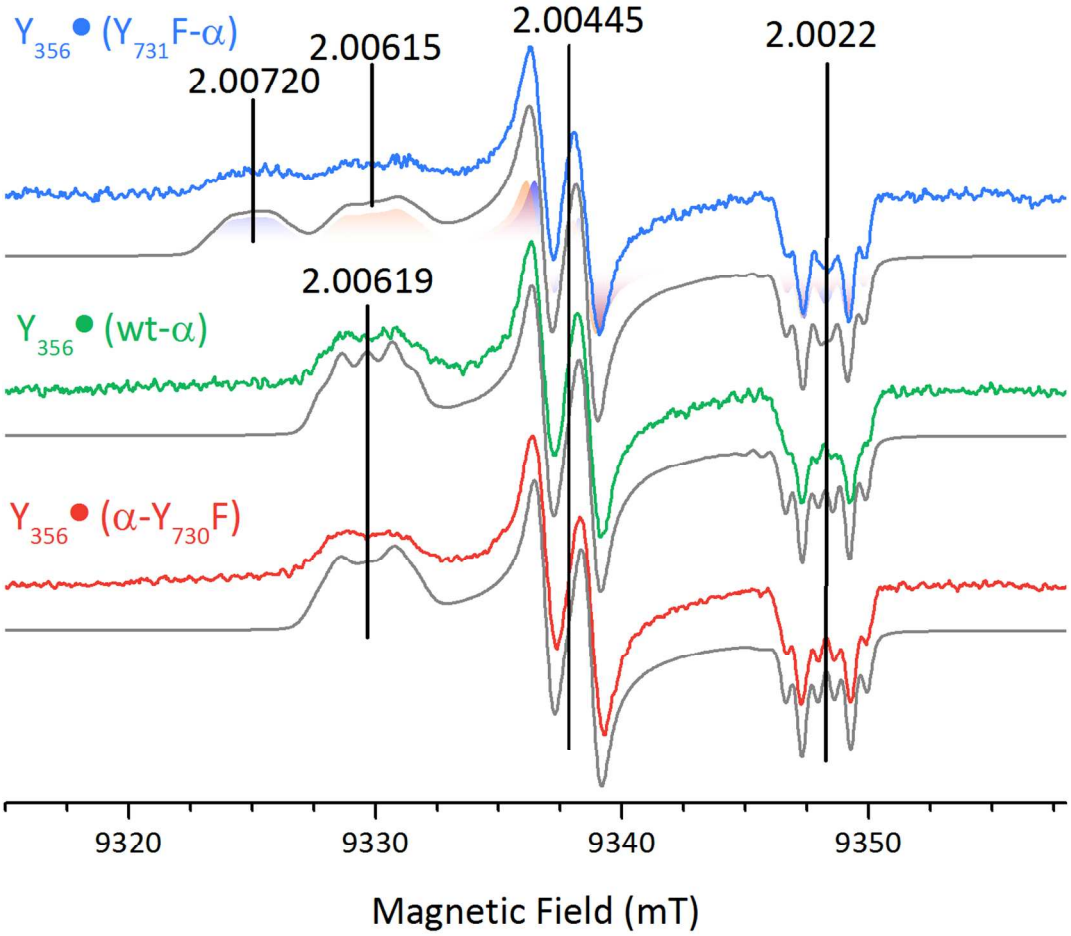

Figure S7: **Multi-frequency simulation of 9 (bottom), 34 (middle) and 94 (top) GHz EPR spectra of Y_{356}•(wt-α).** The experimental spectra and the corresponding simulations are shown in green and grey lines, respectively. The EPR spectra were simulated iteratively to find a global solution for the contributing hf couplings. All of EPR simulations are based on the detected *g*-values from the 263 GHz EPR data shown in Fig. S6. The hf tensors obtained from simulations of the 263 GHz spectra were used as an input for the multifrequency simulation at 9, 34 and 94 GHz. The simulation parameters are shown in **Table S2**. Experimental conditions are as follows: *for 94 GHz*, π=40 ns, *τ*= 270 ns, SRT= 6 ms; *for 34 GHz*, π=40 ns, *τ*= 220 ns, SRT= 5 ms; *for 9 GHz*, power 30 uW, modulation amplitude 1.50 G, modulation frequency 100 kHz, time constant 5.12 ms and scan time 41.93 s. Details of the sample preparation for 94 and 34 GHz experiments are given in *Experimental* in main text and for 9 GHz experiment in Ref. 3. The derivative spectrum was obtained by 3 G pseudo modulation and by a Savitzky-Golay (5 points, second order) filter for 94 and 34 GHz, respectively. A glass tube signal in the 34 GHz spectrum is marked with an asterix.

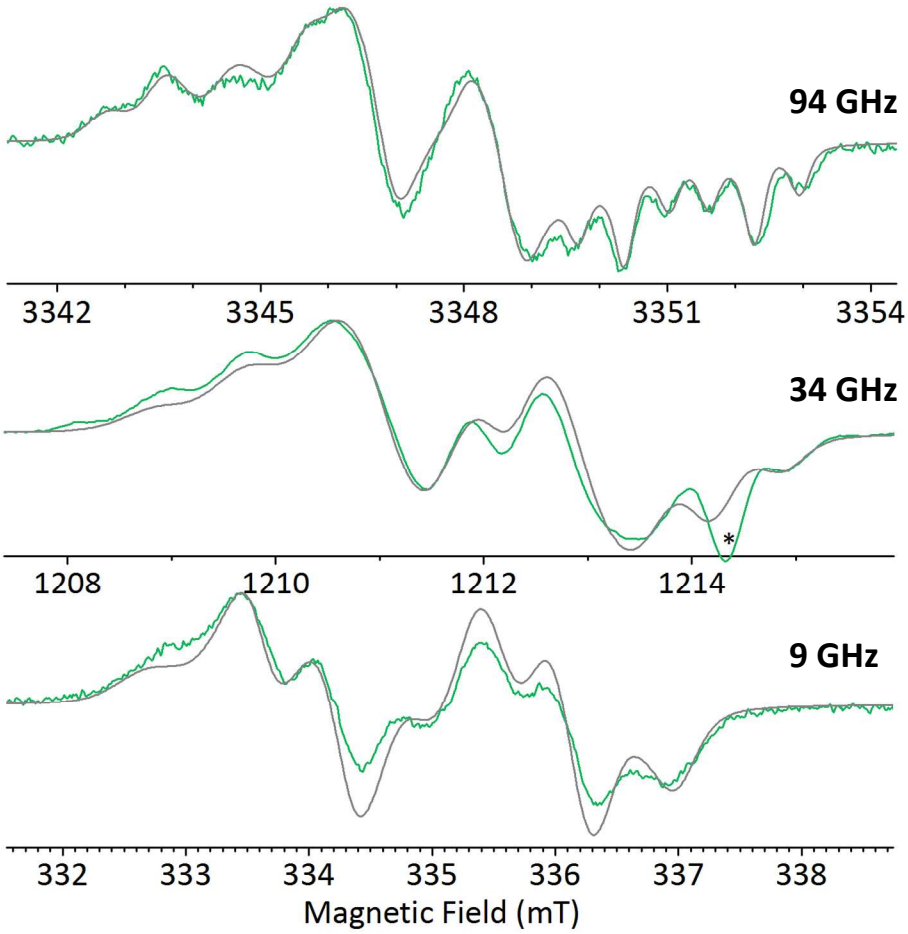

Figure S8: **Multi-frequency simulation of 9 (bottom), 34 (middle) and 94 (top) GHz EPR spectra of Y_{356}•(Y_{731}F-α).** The experimental spectra and the corresponding simulations are shown in blue and grey lines, respectively. The EPR spectra were simulated iteratively to find a global solution for the contributing hf couplings. All of EPR simulations are based on the detected *g*-values from the 263 GHz EPR data shown in Fig. S6. The hf tensors obtained from simulations of the 263 GHz spectra were used as an input for the multifrequency simulation at 9, 34 and 94 GHz. The simulation parameters are shown in **Table S2**. Experimental conditions are as follows: *for 94 GHz*, T=100K; π(π/2)=28 (14) ns; τ =267 ns; SRT = 5 ms; 6000 transients/point; *for 34 GHz*, T=80 K, SRT = 1 ms, π = 40 ns, τ = 210 ns, number of averages = 600; *for 9 GHz*, power 30 uW, modulation amplitude 1.50 G, modulation frequency 100 kHz, time constant 5.12 ms and scan time 41.93 s. Details of the sample preparation for 94 and 34 GHz experiments are given in *Experimental* in main text and for 9 GHz experiment in Ref. 3. The derivative was obtained by 3 G pseudo modulation and by a Savitzky-Golay (8 points, second order) filter for 94 and 34 GHz, respectively. A glas tube signal in the 34 GHz spectrum is marked with an asterix.

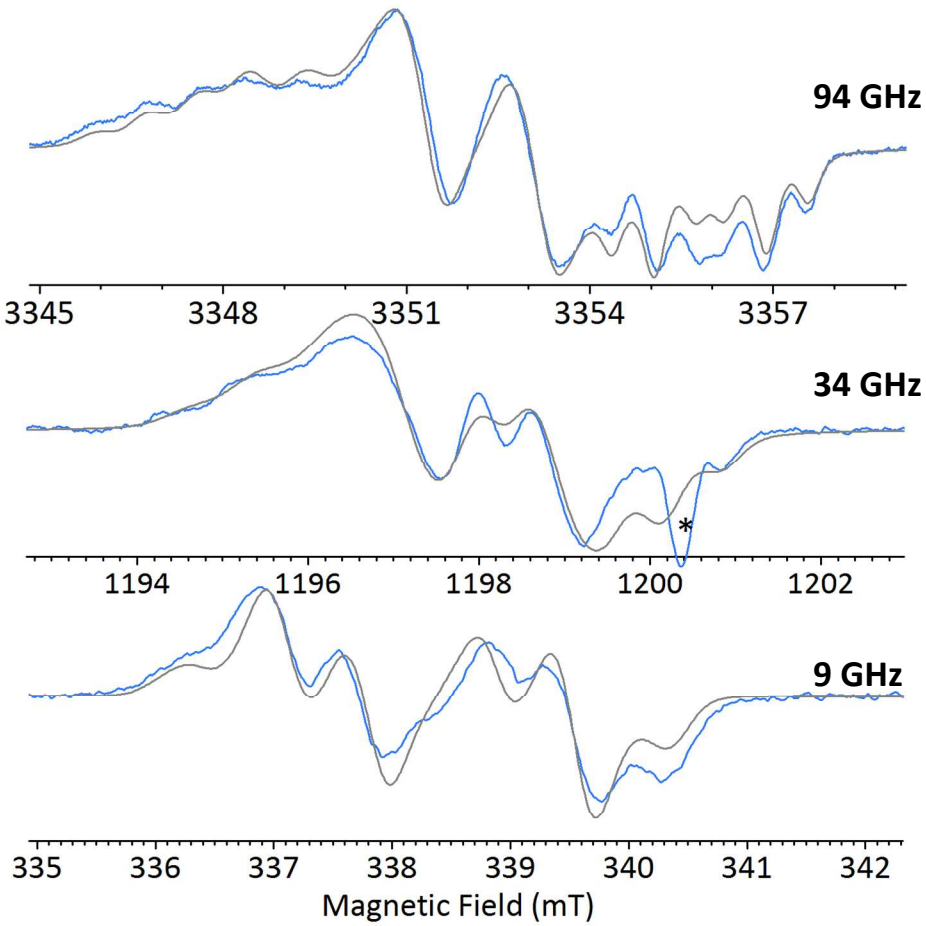

Figure S9: Multi-frequency simulation of 9 (bottom), 34 (middle) and 94 (top) GHz EPR spectra of Y_{356}•(Y_{730}F-α). The experimental spectra and the corresponding simulations are shown in red and grey lines, respectively. The EPR spectra were simulated iteratively to find a global solution for the contributing hf couplings. All of EPR simulations are based on the detected *g*-values from the 263 GHz EPR data shown in Fig. S6. The hf tensors obtained from simulations of the 263 GHz spectra were used as an input for the multifrequency simulation at 9, 34 and 94 GHz. The simulation parameters are shown in **Table S2**. Experimental conditions are as follows: *for 94 GHz*, T=80 K; π(π/2)=44 (22) ns; τ =180 ns; SRT = 3 ms; 2000 transients/point; *for 34 GHz*, T=80 K, SRT = 4 ms, π = 12 ns, τ = 400 ns, number of averages = 1000; *for 9 GHz*, power 30 uW, modulation amplitude 1.50 G, modulation frequency 100 kHz, time constant 5.12 ms and scan time 41.93 s. Details of the sample preparation for 94 and 34 GHz experiments are given in *Experimental* in main text and for 9 GHz experiment in Ref. 3. The derivative was obtained by 3 G pseudo modulation and by a Savitzky-Golay (8 points, second order) filter for 94 and 34 GHz, respectively.

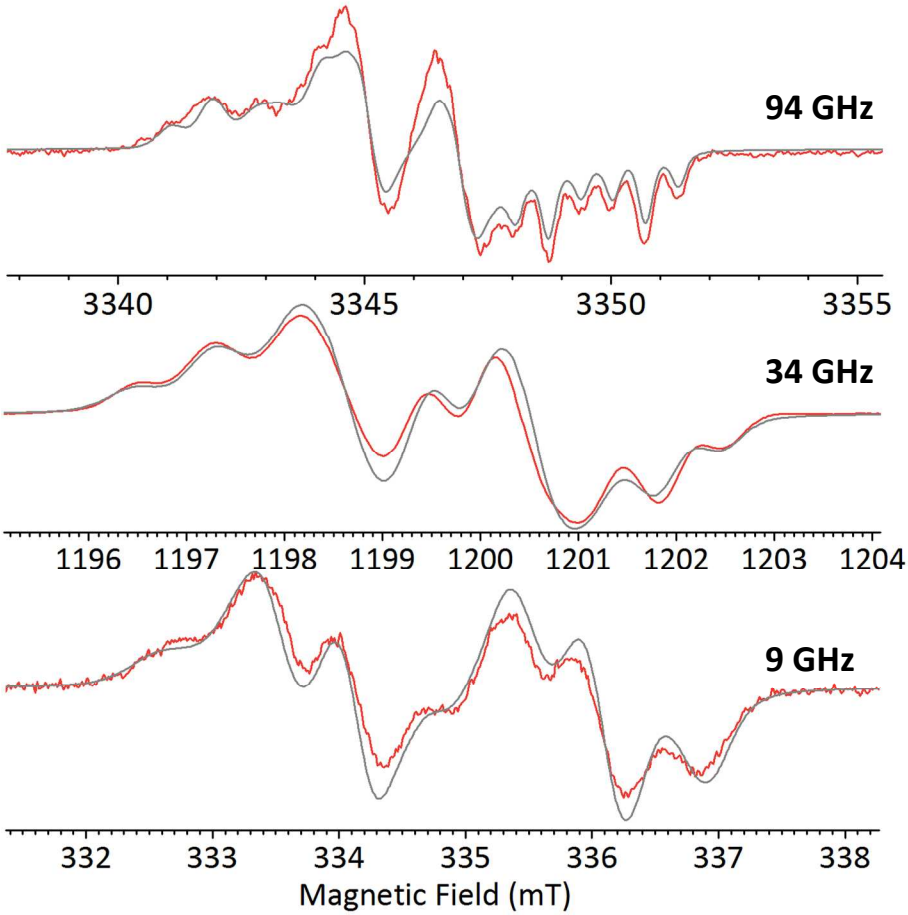

Table S2: Summary of the parameters obtained from multifrequency EPR spectral simulations. Parameters for Y_{356}• generated with wt-α2, Y_{730}F-α2 and Y_{731}F-α2 were obtained from the concomitant simulations of EPR spectra recorded at 9, 34, 94 and 263 GHz. For the simulation of two species observed in Y_{356}•(Y_{731}F-α) parameters of Y_{356}•(Y_{731}F-α) and Y_{356}•(wt-α) were used in a 50:50 mixture. The 2,6-protons and one of the Cβ-protons were not included in the simulation as they are smaller than the inhomogeneous EPR line width of 4 MHz. Hyperfine tensor and *g*-tensor axes were assumed to be collinear for Cβ-protons and Euler angles of [α, β, γ] = [90, 90, ±22] were used for the 3,5-protons.

Y_{356}• (wt-α)			
	g_x	g_y	g_z
g values	2.00619	2.00445	2.0022
g strain	$3\cdot10^{-4}$	$1.5\cdot10^{-4}$	$1\cdot10^{-5}$
HFC	A_1 **(MHz)**	A_2 **(MHz)**	A_3 **(MHz)**
Cβ-^{1}H	52.9	53.9	58.3
C_3-^{1}H	-7	-19.0	29.5
C_5-^{1}H	2.85	18.5	25.5
Y_{356}• (Y_{731}F-α)			
	g_x	g_y	g_z
g values	2.00720	2.00446	2.0022
g strain	$3\cdot10^{-4}$	$1.5\cdot10^{-4}$	$1\cdot10^{-5}$
HFC	A_1 **(MHz)**	A_2 **(MHz)**	A_3 **(MHz)**
Cβ-^{1}H	48	48.5	50.4
C_3-^{1}H	5	20	27.1
C_5-^{1}H	5	19.4	25
Y_{356}• (Y_{730}F-α)			
	g_x	g_y	g_z
g values	2.0062	2.00445	2.0022
g strain	$2\cdot10^{-4}$	$5\cdot10^{-5}$	$1\cdot10^{-5}$
HFC	A_1 **(MHz)**	A_2 **(MHz)**	A_3 **(MHz)**
Cβ-^{1}H	52.9	55.4	62.2
C_3-^{1}H	-7	-19.0	27.5
C_5-^{1}H	2.85	18.5	25.5

Table S3: Dihedral angles between the Cβ-H bond and the p_z orbital axis of C_1 ($\theta_{C\beta}$). The dihedral angles between the Cβ-H bond and the p_z orbital axis of C_1 ($\theta_{C\beta}$) and the C_1 spin population (ρ_{C1}) were extracted from experimental parameters listed in Table S2. We use the algorithm developed by Svistunenko and Cooper[11] based on the McConnel Equation[12]:

$A_{\beta 1} = \rho_{C1}B''\cos^2(\theta)$ and $A_{\beta 2} = \rho_{C1}B''\cos^2(\theta - 120°)$

where B" is 162 MHz. We used the empirical *Tyrosyl Radical Spectral Simulation Algorithm* (TRSSA)[11] to calculate C_1 spin population (ρ_{C1}) based on the experimental g_x values because $A_{\beta 2}$ is not resolved:

$g_x = -0.0359\rho_{C1} + 2.02160$

We note that for Y_{356}•(α-wt), the spin population obtained from the semi-empirical formula at atom C_1 (ρ_{C1}) agrees within the error (20%) with the spin population obtained from the DFT calculation on model 5, that is $\rho_{C1} = 0.375$.

Species	ρ_{C1}	$\theta_{C\beta}$ [°]	$A_{C\beta 1}$ *calculated* [MHz]	$A_{C\beta 1}$ *experiment* [MHz]
Y_{356}• (α-wt): g_x = 2.00619	0.429	27	55	55
Y_{356}• (α-Y_{731}F): g_x = 2.00720	0.401	31	48	48
Y_{356}• (α-Y_{730}F): g_x = 2.0062	0.429	25	57	57

ρ_{C1} Spin densities reported here are on the upper limit of the typically observed range (0.35−0.42) for neutral tyrosyl radicals.[11, 13]

Figure S10: Comparison of Davies ENDOR spectra of [D_6]-Y_{356}•(wt-α) in H_2O and D_2O buffer. The [D_6]-Y_{356}•(wt-α) Davies ENDOR spectrum recorded in D_2O (grey/orange line) and H_2O (green line) buffer. Contribution of non-exchangeable protons is separated by subtracting the ^{1}H ENDOR spectrum of [D_6]-Y_{356}•(wt-α) in D_2O buffer from that of [D_6]-Y_{356}•(wt-α) in H_2O buffer. The subtraction spectrum, which contains only exchangeable H bonds, is shown in grey/blue. Experimental conditions for both spectra are as follows: $\pi_{preparation}$ = 200 ns, SRT= 3 ms, τ = 500 ns, acquisition time = 9 h (green) and 24 h (orange), T= 80 K. The electron spin echo of Y_{356}•(wt-α) in D_2O buffer was more than a factor of two smaller than that of in H_2O buffer. Therefore, the S/N ratio of its ENDOR spectrum was lower in spite of extensive accumulation time. The orange and blue traces were smoothed by 3 points adjacent averaging. Simulation parameters are given in the main text.

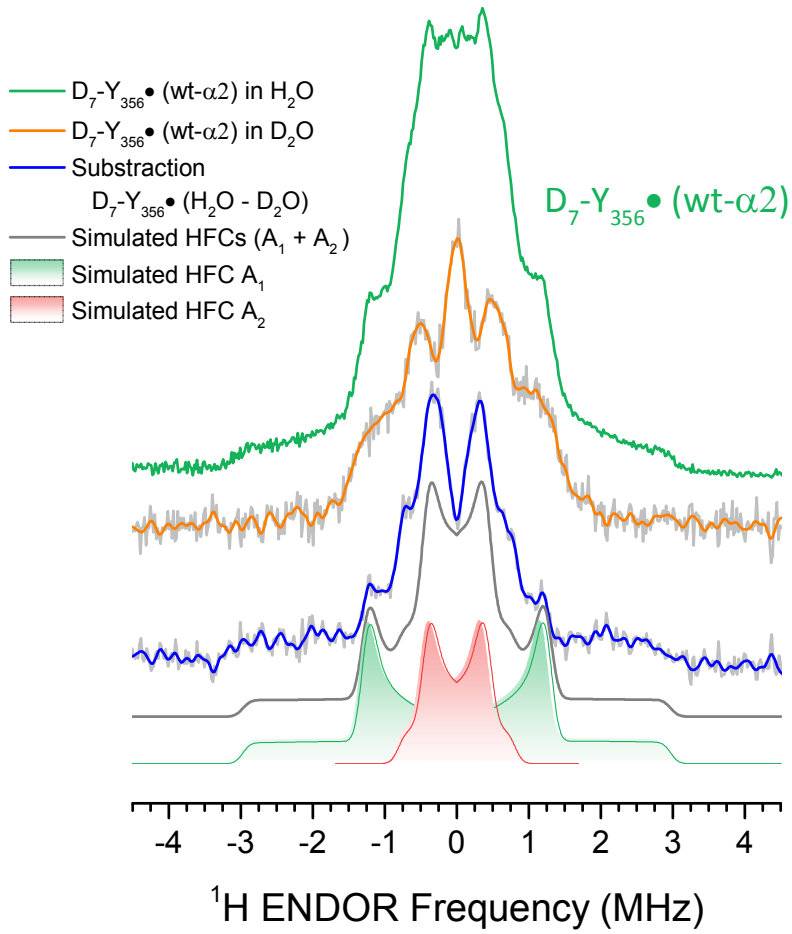

Figure S11: **DFT calculated EPR parameters of a Y• H bonded to one water molecule. A)** The dihedral angle of the H-bond, θ_{OH} (illustrated below), is changed from 0° to 180° systematically and the hf coupling are calculated for each θ_{OH} with the Salt function of Easyspin.[14] The resulting simulations for selected θ_{OH}s are drawn to display the angle dependence of the ENDOR line shape. The restrained geometry scan and the EPR parameter calculation were performed as reported previously on a small Y• model.[15] **B)** Dependence of the calculated g_x on to dihedral angle θ_{OH}.

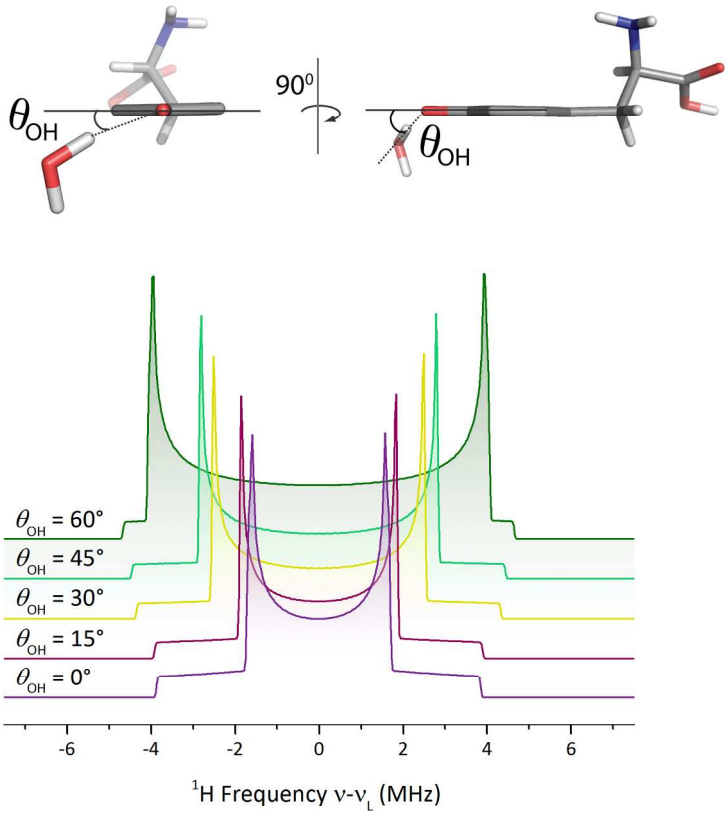

B)

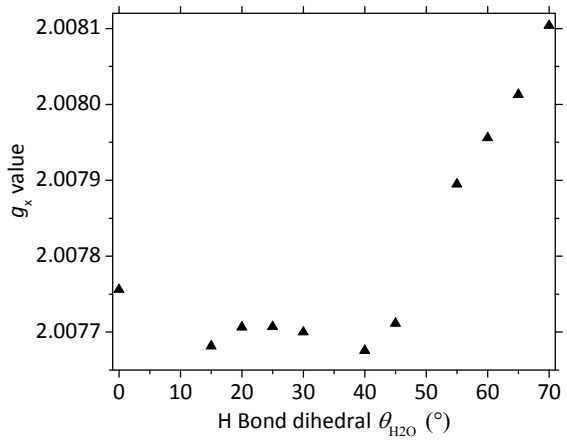

Table S4: Comparison of non-exchangeable proton hf couplings detected and ^{1}H hf couplings calculated for Cα–protons. The largest experimentally observed hf coupling (width of the spectrum) in the ^{1}H ENDOR spectrum of [D_6]-Y_{356}• in D_2O is about 3 MHz and is well consistent with the DFT prediction for the ^{1}H at Cα for the DFT model calculated with two moderate and two weak H bonds (model 5). Notably, the same coupling calculated from model 1, which has one moderate and one single H bond, predicts a larger value. This is due to a subtle shift in spin population distribution on Y_{356}• caused by two *vs.* one moderately coupled water molecules. Note that ^{1}H at Cα, which resides on the Y backbone, is not relevant for the observed g_x-shift that requires electrostatic interactions at the phenolic oxygen.

Model	Hf coupling (A_z) of ^{1}H at Cα from DFT (MHz)
Model 1	-4.9
Model 5	-3.5

Figure S12: Comparison of ^{1}H-Davies and ^{2}H-Mims ENDOR spectra of Y_{356}•(wt-α) at 34 GHz and simulation of ^{2}H-Mims ENDOR spectrum with two moderate H-bonds. We compared the ^{2}H Mims ENDOR spectra of Y_{356}•(wt-α) generated in D_2O buffer (green) ^{1}H Davies ENDOR spectra of [D_6]-Y_{356}•(wt-α) generated in H_2O buffer (black). The ^{2}H frequency axis is scaled to the ^{1}H spectra (^{2}H frequency times 6.5) to display the correspondence in the observed hf couplings. Moreover, the observed resonances in the black spectrum are split into two due to the presence of quadrupole couplings ($Q_{x,y,z}$). The green spectrum was simulated with two deuteriums having similar hf coupling constants, D_1 and D_2, which are similar to A_1 detected in this work. The size of the hyperfine and quadrupole coupling constants revealed by our simulations are in agreement with the ones reported previously for the stable Y• in yeast RNR[16] and Y_D• in photosystem II (PSII).[17] The H bond distances to the Y• in yeast RNR and PSII, which were 1.8 Å, are similar to the ones revealed by our DFT calculations for model 5 (Table 2 in main text). Furthermore, the dihedral angle θ_{OH} between the H-bond direction and the tyrosine plane was found to be 20° in yeast RNR and 17° in PSII. These numbers are also similar with our DFT calculations that revealed θ_{OH} of 21° and 12° for the two H bonds. Simulations of the individual deuterium couplings D_1 and D_2 and the combination of the two, D_1 + D_2, are shown with purple, dark gray and gray lines, respectively. Simulation parameters are given below. The spectra are centered at the Larmor frequency of $^{1/2}$H, ν_0 = 51.2 and 7.8 MHz at 1.2 T. Experimental conditions: Mims ENDOR (green line): $\pi/2$ = 6 ns, SRT= 5 ms, τ = 300 ns, acquisition time = 24 h, T= 80 K; Davies ENDOR (black line): π_{prep} = 200 ns, τ = 500 ns, SRT = 3 ms, acquisition time = 54 h, T= 80 K.

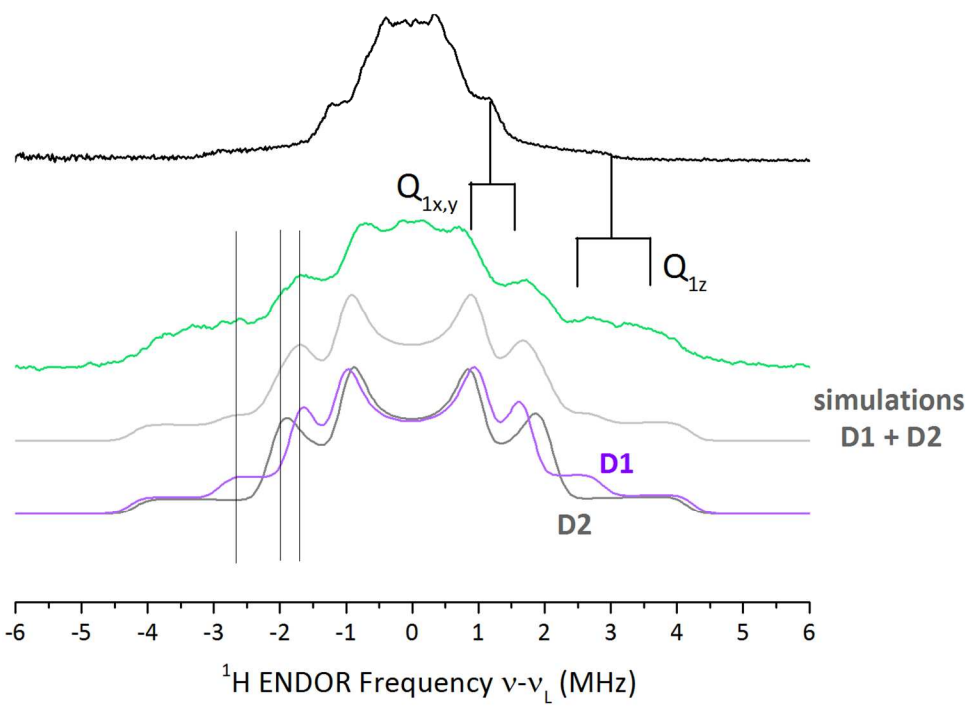

Simulation parameters:

Y_{356}•(wt-α)	Hf couplings [MHz]			Quadrupole couplings [kHz]		
	A_x	A_y	A_z	Q_x	Q_y	Q_z
D_1	-0.43	-0.45	1.1	-0.025	-0.035	0.08
D_2	-0.45	-0.48	0.95	-0.047	-0.064	0.11

Figure S13: Orientation selective ^{2}H Mims ENDOR spectra of Y_{356}• (wt-α) at 94 GHz. Black dashed lines mark hf splittings $A_{x,y}$ as assigned at B||g_z as well as the largest splitting observed at this orientation (gray dashed lines). The ^{2}H spectra contain also additional quadrupole splittings as illustrated in **Fig. S12**. Left inset shows the *g* and A tensor directions for a hydrogen bond in plane with the Y• ring. The right inset shows the EPR line shape at 94 GHz and the excitation bandwidth at the three canonical orientations of the *g* tensor in the EPR line. Experimental conditions: π/2=36 ns, *τ*=300-400 ns, π_{RF}= 40 µs, random RF acquisition with 1 shots/point, SRT = 5-10 ms, acquisition time = 40 h/spectrum, 80 K, shot repetition time = 10 ms. The raw data was processed by 10 point adjacent averaging.

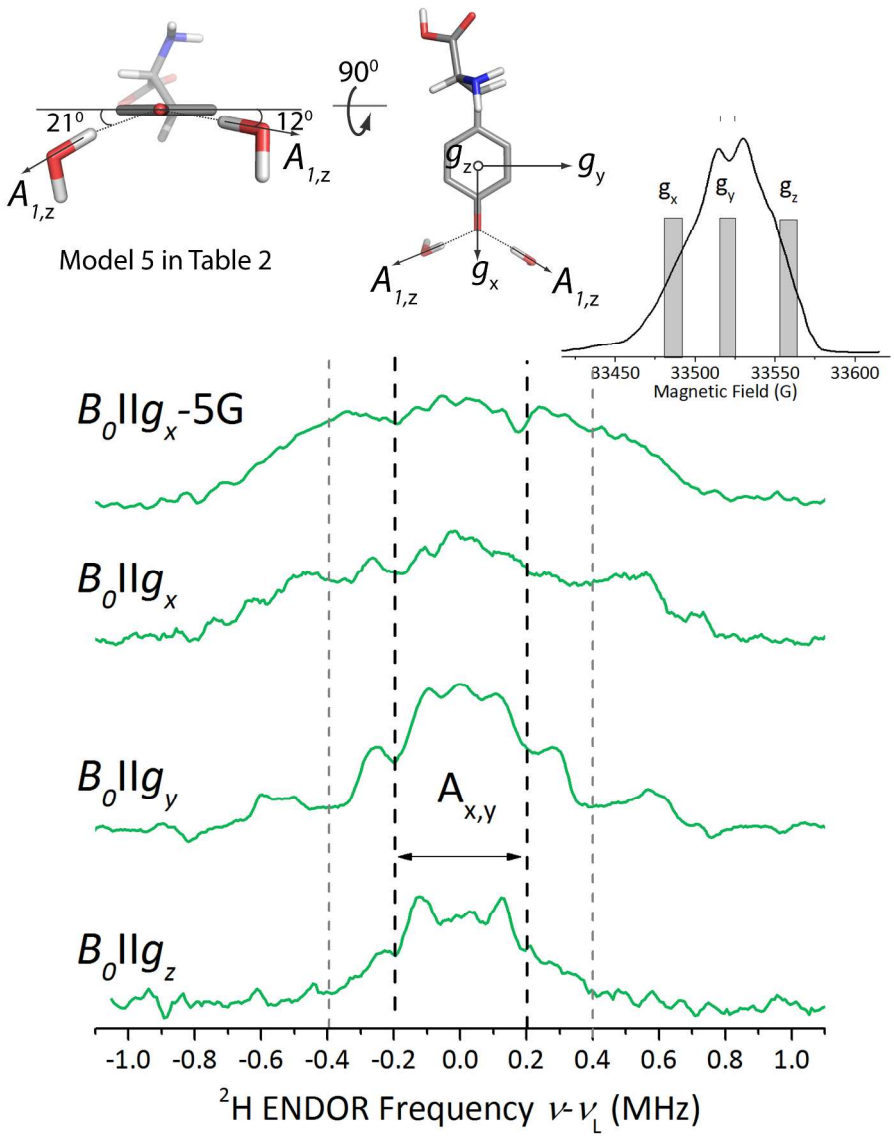

References

(1) Minnihan, E. C., Young, D. D., Schultz, P. G., and Stubbe, J. (2011) *J. Am. Chem. Soc. 133*, 15942-15945.

(2) Oyala, P. H., Ravichandran, K. R., Funk, M. A., Stucky, P. A., Stich, T. A., Drennan, C. L., Britt, R. D., and Stubbe, J. (2016) *J. Am. Chem. Soc. 138*, 7951-7964.

(3) Ravichandran, K. R., Minnihan, E. C., Wei, Y., Nocera, D. G., and Stubbe, J. (2015) *J. Am. Chem. Soc. 137*, 14387-14395.

(4) Seyedsayamdost, M. R., and Stubbe, J. (2009) In *Methods Enzymol.* , Vo. 462, pp 45-76 (Tom, W. M., and John, N. A., Eds.), Academic Press.

(5) Nick, T. U., Lee, W., Koßmann, S., Neese, F., Stubbe, J., and Bennati, M. (2015) *J. Am. Chem. Soc. 137*, 289-298.

(6) Jeschke, G., Chechik, V., Ionita, P., Godt, A., Zimmermann, H., Banham, J., Timmel, C. R., Hilger, D., and Jung, H. (2006) *Appl. Magn. Reson. 30*, 473-498.

(7) Tikhonov, A. N. (1995), Kluwer Academic Publishers, Dordrecht; Boston.

(8) Seyedsayamdost, M. R., Chan, C. T. Y., Mugnaini, V., Stubbe, J., and Bennati, M. (2007) *J. Am. Chem. Soc. 129*, 15748-15749.

(9) Yokoyama, K., Smith, A. A., Corzilius, B., Griffin, R. G., and Stubbe, J. (2011) *J. Am. Chem. Soc. 133*, 18420-18432.

(10) Bennati, M., Weber, A., Antonic, J., Perlstein, D. L., Robblee, J., and Stubbe, J. (2003) *J. Am. Chem. Soc. 125*, 14988-14989.

(11) Svistunenko, D. A., and Cooper, C. E. (2004) *Biophys. J. 87*, 582-595.

(12) McConnell, H. M., and Chesnut, D. B. (1958) *J. Chem. Phys. 28*, 107-117.

(13) Stoll, S. (2011) High-field EPR of bioorganic radicals, In *Electron Paramagnetic Resonance.* Roy. Soc. of Chem. *Vol. 22*, pp 109-122,

(14) Stoll, S., and Schweiger, A. (2006) *J. Magn. Reson. 178*, 42-55.

(15) Kasanmascheff, M., Lee, W., Nick, T. U., Stubbe, J., and Bennati, M. (2016) *Chem. Sci. 7*, 2170-2178.

(16) Bar, G., Bennati, M., Nguyen, H. H. T., Ge, J., Stubbe, J., and Griffin, R. G. (2001) *J. Am. Chem. Soc. 123*, 3569-3576.

(17) Keßen, S., Teutloff, C., Kern, J., Zouni, A., and Bittl, R. (2010) *ChemPhysChem 11*, 1275-1282.